J. Fluid Mech. (2002), *vol.* 468, *pp.* 77–105.
DOI: 10.1017/S0022112002001593 Printed in the United Kingdom

Effect of preferential concentration on the settling velocity of heavy particles in homogeneous isotropic turbulence

By A. ALISEDA, A. CARTELLIER†, F. HAINAUX AND J. C. LASHERAS

Department of Mechanical and Aerospace Engineering, University of California San Diego, La Jolla, CA 92093, USA

(Received 26 July 2001 and in revised form 16 April 2002)

The behaviour of heavy particles in isotropic, homogeneous, decaying turbulence has been experimentally studied. The settling velocity of the particles has been found to be much larger than in a quiescent fluid. It has been determined that the enhancement of the settling velocity depends on the particle loading, increasing as the volume fraction of particles in the flow increases. The spatial and temporal distribution of the particle concentration field is shown to exhibit large inhomogeneities. As the particles interact with the underlying turbulence they concentrate preferentially in certain regions of the flow. A characteristic dimension of these particle clusters is found to be related to the viscous scales of the flow. Measurements of the settling velocity conditioned on the local concentration of particles in the flow have shown that there is a monotonic increase in the settling velocity with the local concentration (the relation being quasi-linear). A simple phenomenological model is proposed to explain this behaviour.

1. Introduction

The evolution of particle-laden flows is relevant to many industrial and environmental processes. Some examples are the flow in chemical reactors and combustion chambers, cloud dynamics, deposition of sediments on river banks, dust storms, etc. The behaviour of heavy particles or droplets in a turbulent flow has been thoroughly investigated over the past few years, see Snyder & Lumley (1971), Maxey & Riley (1983), Lázaro & Lasheras (1992*b*), Schreck & Kleis (1993), Kulick, Fessler & Eaton (1994), Crowe, Troutt & Chung (1996), among others. There are, however, a number of issues that are still not well understood, the most important being the effect of the turbulence on the concentration field and on the settling of the particles, as well as the modification of the carrier flow turbulence due to the presence of the particles.

It has been known for a long time that particles immersed in a turbulent flow tend to accumulate, creating large inhomogeneities in the concentration field. This preferential accumulation of particles in a turbulent flow has traditionally been explained by the inertial bias mechanism. When a particle that is heavier than the surrounding fluid interacts with a vortex, or a turbulent structure, the particle is accelerated in the outward direction by centrifugal forces. Auton, Hunt & Prud'Homme (1988), Gañán-Calvo & Lasheras (1991), Ruetsch & Meiburg (1993), Tio, Gañán-Calvo & Lasheras

† On leave from: LEGI, CNRS/UJF/INPG, Grenoble, France.

(1993), Lasheras & Tio (1994), among others, have analysed this effect for particles interacting with vortices of different types. Studies of the trajectories of particles settling in a cellular flow, Maxey (1987*a*), and in a flow created by random vortices that follow a prescribed, turbulence-like spectrum, Maxey (1987*b*), have shown this preferential concentration of heavy particles in regions of low vorticity and high strain rate. Finally, direct numerical simulations (DNS) of particle-laden flows have confirmed that, as the particles interact with the fluctuating velocity field of the carrier flow, they accumulate in regions of low vorticity and high strain, leading to an inhomogeneous, intermittent concentration field, see Squires & Eaton (1991), Wang & Maxey (1993), Truesdell & Elghobashi (1994), Yang & Lei (1998) and Février, Simonin & Legendre (2001). For a review of the most significant results on the preferential concentration of particles by turbulence, the reader is referred to the article by Eaton & Fessler (1994).

In the presence of gravity, heavy particles have a vertical velocity with respect to the surrounding fluid. Along its trajectory, every particle interacts with different vortices and the crossing trajectories effect causes the particle to be preferentially swept to the downward side of the eddies. Thus, the mean effect of the turbulence on a particle is a net force that accelerates it downwards. Wang & Maxey (1993) studied this phenomenon by direct numerical simulation of particles interacting with homogeneous isotropic turbulence and found an increase in the settling velocity of particles in a turbulent flow, even when particles have no effect on the carrier flow (one-way coupling) and particles are only affected by the drag due to the local velocity of the carrier flow. When the particles are considered as point forces that exert a force on the fluid equal to the drag the fluid exerts on them but with opposite sign (a limited form of two-way coupling), carrier turbulence is not significantly modified, as long as the volumetric and mass loading of particles are low enough, see Elghobashi & Truesdell (1993), Boivin, Simonin & Squires (1998), Druzhinin & Elghobashi (1999) and Sundaram & Collins (1999). The settling velocity of particles in a turbulent flow is enhanced due to the interaction of the particles with the turbulent structures. For particles in the size range studied and in homogeneous isotropic turbulence, the most significant interaction is believed to be at the level of the smallest structures of the turbulence, namely at the Kolmogorov scales. The spatial distribution of particles in the flow is also influenced by these turbulent structures.

Both particle accumulation and enhanced settling due to turbulence have been found to depend primarily on two non-dimensional parameters, namely the Stokes number and the terminal velocity ratio, Wang & Maxey (1993). The Stokes number is defined as a ratio between the viscous relaxation time of the particle and a turbulent time scale, and represents the effect of the particle inertia in the interaction with the turbulence $St = \tau_p/\tau_k$. The choice of the appropriate fluid time scale has been a matter of controversy in the past, but following Wang & Maxey (1993) we will use the Kolmogorov time scale τ_k. This represents the turnover time of the eddies in the smallest scales of the turbulence, which is where the basic interaction with the particles is expected to occur. The characteristics times are defined as follows:

$$\tau_p = \frac{d^2 \rho_p / \rho_{air}}{18 \nu_{air}}, \quad \tau_k = \left(\frac{\nu_{air}}{\epsilon}\right)^{1/2}, \tag{1.1}$$

where d is the diameter of the particle, ρ_p and ρ_{air} are the dispersed and continuous phase densities, ν_{air} is the kinematic viscosity of the continuous phase and ϵ is the dissipation rate of turbulent kinetic energy in the flow. The terminal velocity ratio compares the importance of the terminal velocity of the particles to a characteristic

velocity of the turbulence, measuring the residence time of a particle in an eddy, in eddy turnover time units. Thus, it quantifies the importance of the crossing trajectories effect. Again, the Kolmogorov microscale is chosen in accordance with the previous reasoning. This velocity ratio can be related to the Stokes number by

$$\frac{V_t}{v_k} = \frac{\tau_p}{\tau_k} \frac{g}{(\epsilon^3/\nu_{air})^{1/4}}, \tag{1.2}$$

showing that, for a given fluid and turbulence dissipation rate, these two non-dimensional parameters are not independent and both phenomena can be characterized by only one of them.

Due to the complexity involved in the experimental characterization of particle-laden flows, most of the recent progress on the behaviour of heavy particles in homogeneous turbulent flows has come from numerical simulations. The lack of experimental results to support the evidence produced by numerical simulation complicates the distinction between the behaviour due to the interaction of particles and turbulence and the spurious effects introduced in the numerical simulations. In this context, we set out to build an experiment where heavy particles could be injected into a homogeneous, isotropic decaying turbulent flow. Data taken under these well-controlled conditions can provide valuable insight into the behaviour of particles in real turbulent flows, at least in regions where the turbulence can be considered to be homogeneous and isotropic. In particular, we will concentrate our attention on the modification of the particle settling velocity due to its interaction with the turbulent flow and on the preferential accumulation effects resulting from the particle–turbulence interaction.

The structure of the paper is as follows. In § 2 we describe the experimental set-up, as well as the different experimental techniques used. Measurements of the particle settling velocity for various particle mass loadings are given in § 3. In addition, measurements of the spatial distribution of the particle concentration field are also presented in § 3, and are used to determine the characteristic size of the particle clusters. The data analysis and comparison with the previous work is given in § 4. In § 5 we discuss a simple phenomenological model of particle clusters in turbulent flows, as a first-order attempt to quantitatively explain the discrepancy in the settling velocity between the experimental results and the numerical simulations, via a new added effect of turbulence on the settling velocity of heavy particles. Finally, the conclusions are summarized in § 6.

2. Experimental set-up

The experiments were performed in a horizontal blow-down wind tunnel, with a test section length of 2.5 m and a square cross-section of 20 cm by 20 cm. The air flow is laden with water droplets injected upstream of the test section. A sketch of the facility is shown in figure 1. The air flow is supplied by a blower and passes through a nozzle, with an area contraction ratio of 2 : 1. Fine mesh screens and honeycombs are also used to damp out all possible inhomogeneities in the flow before entering the test section. The turbulence is produced by a grid in which the liquid atomizers are embedded. The grid is made up of round tubes, with a diameter of 1 mm and a lateral spacing M of 15 mm.

Water droplets are injected in the air stream through an array of atomizers embedded in the vertical bars of the grid, producing a uniform spray over the central region of the tunnel (14 cm by 14 cm). Each atomizer, a sketch of which is shown

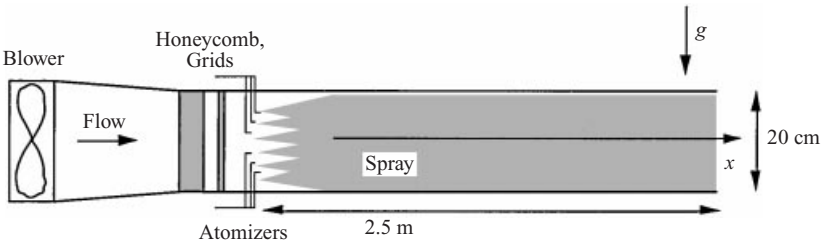

FIGURE 1. Experimental facility.

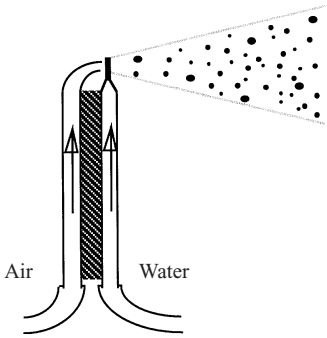

FIGURE 2. Sketch of an atomizer used in the experiment.

in figure 2, consists of two parallel tubes carrying water and air. The water is delivered normal to the main flow while the pressurized air exits the nozzle parallel to the main stream. The high-momentum air jet impinges perpendicularly on the water jet, atomizing the liquid and producing a spray jet. The droplet size distribution and liquid mass fraction of the spray can be controlled by the pressure of the air supply line and by the flow rate of water, as shown by Lázaro & Lasheras (1992*a*). In all the experiments reported here the air pressure was kept constant, while the water flow rate was varied over a range where its influence on the resulting droplet size distribution was negligible. Additionally, the droplet size distribution was measured at different locations along the test section and found to be uniformly the same. This allowed us to discard coalescence and breakup effects in all the experiments. The droplet size distribution used through all the experiments reported here is shown in figure 3. The droplet turbulent Weber number, $We_t = \rho_p \overline{u(d)^2} d/\sigma$, is always less than 10^{-2} for all droplets in the distribution. Thus, surface tension dominates over the unsteady pressure distribution from the gas that may deform the droplets, allowing us to assume a spherical shape for the droplets during the experiments.

The characteristics of both the single-phase turbulent carrier flow and the injected droplets were carefully determined by hot-wire anemometry and phase Doppler particle analysis (PDPA) and the region of the flow where wall effects could be neglected was identified. Several iterations of changes in the geometry and the operating conditions of the experiment were necessary to ensure that the conditions selected corresponded to nearly homogeneous, isotropic, slowly decaying turbulent particle-laden flow.

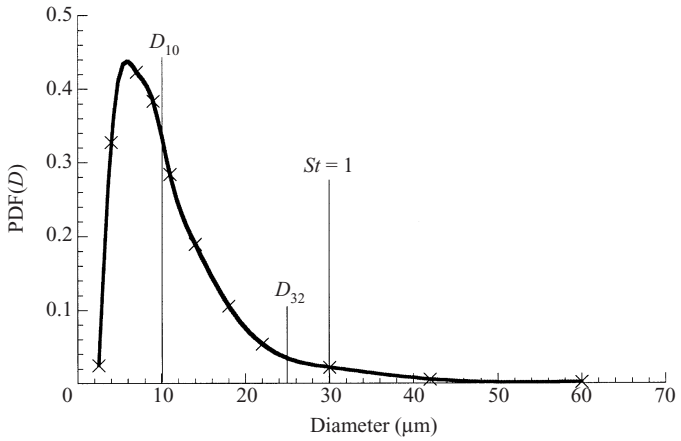

FIGURE 3. Probability density function of the droplet's diameter.

2.1. *Turbulence characterization*

The characteristics of the turbulence of the single-phase air flow were determined by hot-wire constant-temperature anemometry. An AA Lab Systems AN-1003 anemometer with a TSI, 1210-T1.5, single wire probe were used, together with a National Instruments BNC 2090 digital acquisition card. Information was acquired at a frequency of 10 kHz, which is fast enough to resolve the dissipation range of the turbulent spectrum. The length of each individual data set was 5×10^5 samples (or 50 s), and the statistically stationary flow hypothesis was checked by comparing the results with data sets which were 2.5×10^5 and 10^6 points long. The data were then processed to compute the turbulent characteristics. The selected flow has a bulk Reynolds number ($Re = U_\infty l/v$) of 7.5×10^4 and a Reynolds number based on the Taylor microscale of $Re_\lambda = 75$.

It was observed that the air injected through the atomizers contributed significantly to both the total momentum (up to 10%) and the initial value of the turbulent intensity of the carrier flow (up to 50%). Therefore, the characterization of the turbulence was done with the atomizers injecting air at their normal operating conditions. The fact that the injection of air contributes significantly to the turbulence intensity made the grid of atomizers an active grid, potentially modifying the decaying characteristics of the turbulence produced by it.

Measurements were taken at six downstream locations, over a set of 16×6 points in the z- and y-directions with a spacing of 1 cm, covering the central part of the wind tunnel. The measuring region extended from $x = 83$ cm to $x = 207$ cm (see the sketch in figure 4). Measurements showed that the flow could be considered to be homogeneous in planes perpendicular to the axial velocity (y, z-planes). Vertical profiles of the mean axial velocity (U) are shown in figure 5. Although the growth of the boundary layer can be observed in figure 5(b), the selected region of interest for our experiments is located well outside its limits. Thus, within the test section relevant for our experiments, the flow can be assumed to be unaffected by the presence of the walls. Vertical profiles of the axial velocity RMS (u') are shown in figure 6. Again, the effect of the boundary layer is found to be restricted to a region far away from the measuring zone.

In order to characterize the decay of the turbulence, the inverse of the turbulent kinetic energy can be fitted to a power law. Comte-Bellot & Corrsin (1966) proposed an exponent of between 1.2 and 1.3 to best fit the data over the whole range. It has

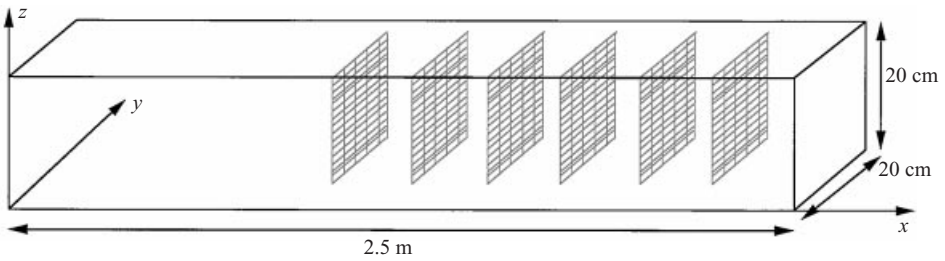

FIGURE 4. Sketch of hot-wire measurement locations.

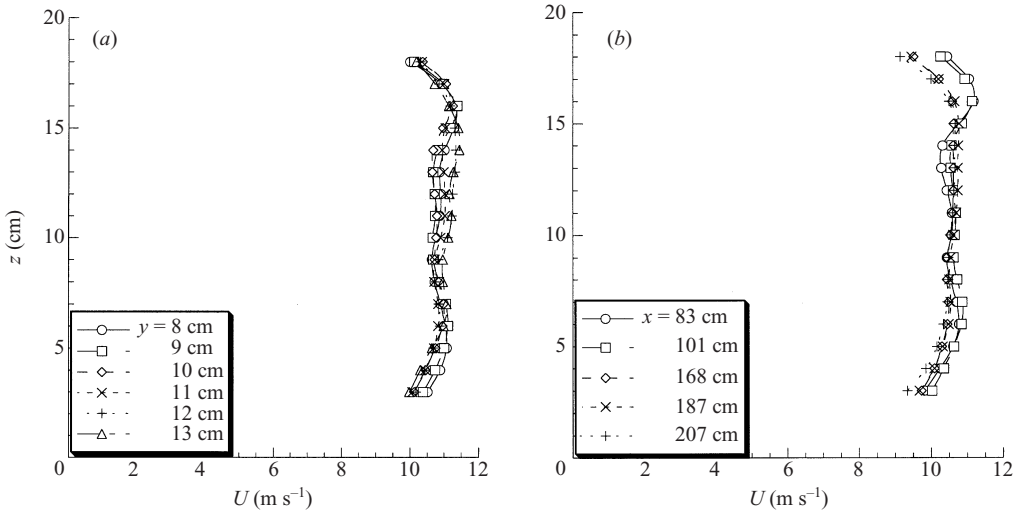

FIGURE 5. (*a*) Mean axial velocity profiles ($x = 101$ cm). (*b*) Downstream evolution of the mean axial velocity at the centre of the tunnel.

been further proposed, Wells & Stock (1983), that three different regions of decay can be identified in grid-induced turbulence. The near region, which extends from 10 to 150 mesh distances downstream from the grid, is characterized by a decay of the turbulent intensity proportional to the inverse of the distance downstream. In the far region, which extends from 500 mesh lengths onwards, the decay of the turbulent intensity is faster and is given by $(U/u')^2 \sim (x - x_0)^{5/4}$, where x_0 is the virtual origin in the turbulent decay curve. There is also some evidence of an intermediate region where the turbulent intensity decays as $(U/u')^2 \sim (x - x_0)^{10/7}$.

The decay of the turbulent intensity measured at the centreline of the tunnel is shown in figure 7. Since all of our data lie well within the near region and the macroscale Reynolds number is almost constant, it is justified to apply a linear fit to our data, $(U/u')^2 = 38.41(x/M - 10.17)$. Thus characterized, we have the means to compare the decay law for the active grid in our experiment with those of passive grids.

Since the typical time scale of the decay of the turbulence is much larger than the particle's response time, we will assume quasi-stationary conditions when analysing the problem of the interaction of the particles with the turbulence. Following Nir & Pismen (1979), the time of decay of the turbulence as seen by a particle moving with the mean streamwise velocity of the flow can be estimated by $t_d^{-1} = U\,\mathrm{d}\ln(u')/\mathrm{d}(x - x_0)$. In all our experiments, this time is of the order of 0.2 s, which is much larger than

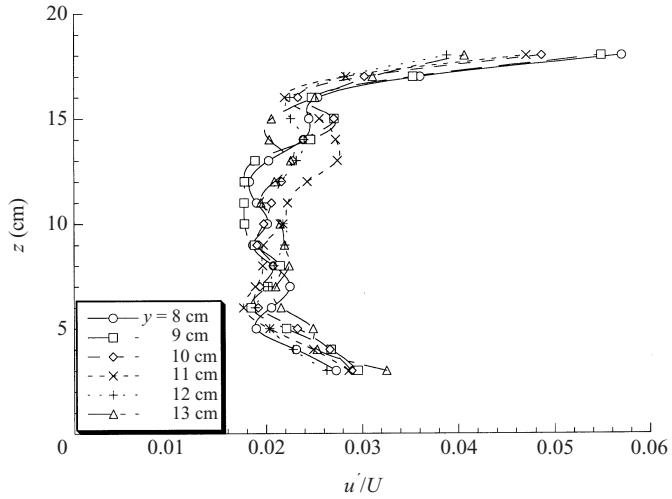

FIGURE 6. Turbulent intensity profiles ($x = 101$ cm) at different vertical sections of the tunnel.

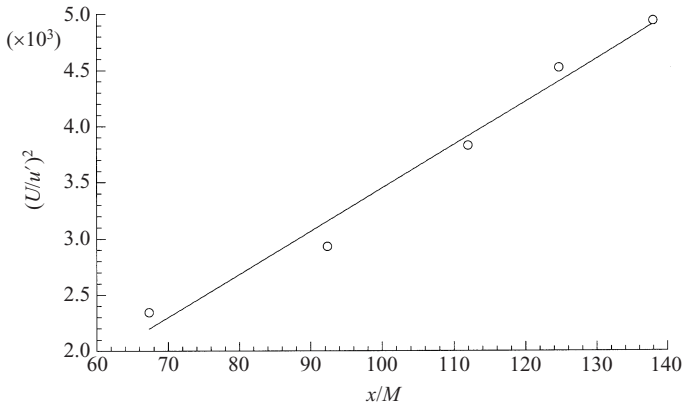

FIGURE 7. Decay of the turbulent intensity along the test section.

the response time of all particles. Thus, we can assume that the particles are always in equilibrium with the surrounding turbulence.

The one-dimensional power spectrum of the carrier fluid (air flow) was computed at all downstream locations in the tunnel, using a fast Fourier transform algorithm. The spectrum, plotted in figure 8, shows the typical features of a moderate Reynolds number flow, including a very short inertial subrange of less than a decade.

The turbulence characteristics obtained from the hot-wire measurements are shown in table 1. The dissipation rate of turbulent kinetic energy ϵ was computed with two different methods as an integral of the unidirectional spectrum, (2.1), and from the derivatives of the fluctuating velocities, (2.2), Hinze (1975). Both calculations were found to agree to within 10% for all downstream locations:

$$\epsilon = 15\nu \int_0^\infty k^2 E_{11}(k)\,\mathrm{d}k, \tag{2.1}$$

$$\epsilon = -\frac{1}{2}\frac{\mathrm{d}\bar{q}^2}{\mathrm{d}t}. \tag{2.2}$$

x (cm)	u' (cm s^{-1})	ϵ (m^2 s^{-3})	L (mm)	λ (mm)	η (mm)	τ_k (ms)	v_k (cm s^{-1})
83	26.2	1.75	37.7	5.06	0.210	2.92	7.16
101	21.1	1.00	43.0	5.37	0.241	3.87	6.23
138	19.6	0.88	48.4	5.26	0.249	4.13	6.03
168	17.6	0.76	50.5	4.80	0.258	4.43	5.82
187	16.3	0.68	56.5	4.64	0.265	4.69	5.66
207	15.6	0.61	56.2	4.66	0.273	4.96	5.50

TABLE 1. Downstream evolution of the turbulence characteristics for the single-phase air flow: distance downstream, x; velocity RMS, u'; turbulent dissipation, ϵ; integral length scale, L; Taylor length scale, λ; Kolmogorov microscale, η; Kolmogorov time scale, τ_k; Kolmogorov velocity scale, v_k.

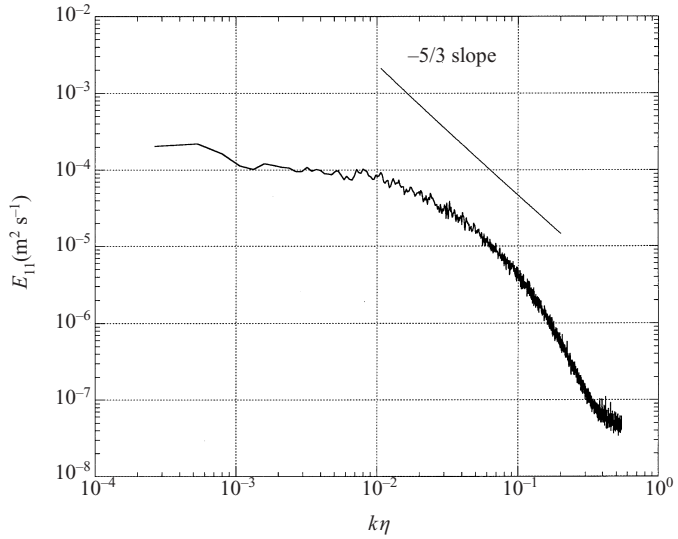

FIGURE 8. Longitudinal one-dimensional turbulent energy spectrum.

The Kolmogorov microscales were computed from their definitions, $\tau_k = (\nu/\epsilon)^{1/2}$, $\eta = (\nu^3/\epsilon)^{1/4}$, $v_k = (\nu\epsilon)^{1/4}$. It is important to notice that the Kolmogorov length scale in the carrier flow is an order of magnitude larger than the droplet diameter (both the arithmetic and Sauter mean diameters).

To characterize the isotropy of the carrier gas, measurements of the RMS of the velocity of the flow in the three directions are needed. Measurements of the velocity in the x- and z-directions were taken with the phase Doppler particle analyser system (PDPA), described in §2.2. For this purpose, the flow was seeded with very small smoke particles ($d < 1\,\mu$m), which behave as fluid elements, and their horizontal and vertical velocities were processed to obtain the values of u' and w'. As a test of the accuracy of this procedure, it should be noted that the value of u' obtained from the PDPA measurements agrees very well with the one we measured using the hot-wire technique. In figure 9, we plot the ratio of u' and w', showing that it remains very close to unity, with a maximum deviation of less than 10%. In addition, the probability density function (PDF) for the fluctuating velocity, shown in figure 10, was found to be nearly Gaussian.

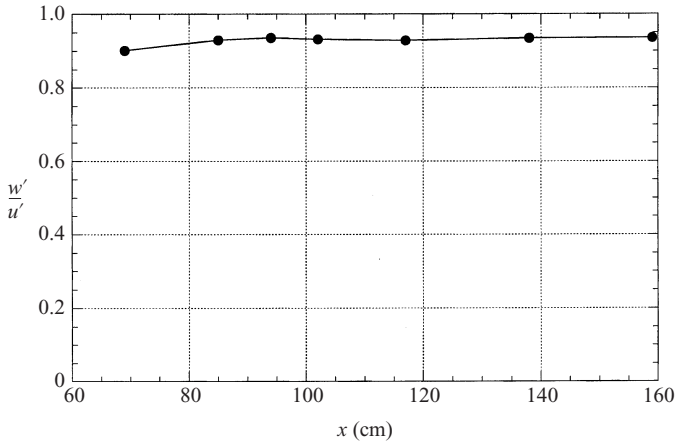

FIGURE 9. Ratio of the RMS of the horizontal and the vertical velocities.

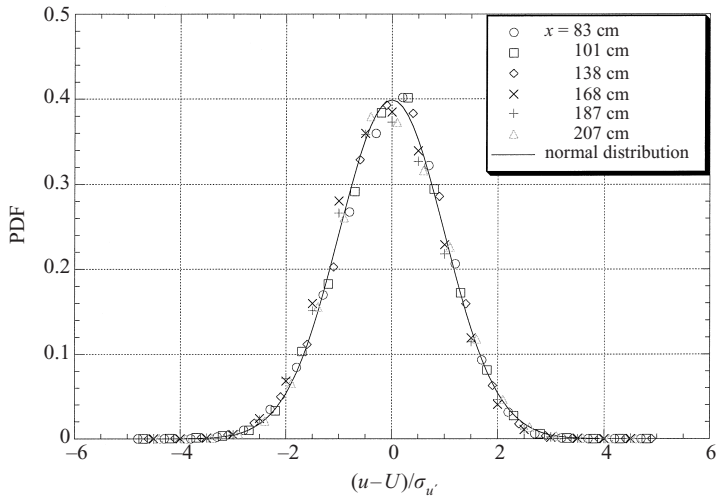

FIGURE 10. Probability density function of the fluctuating velocity.

2.2. *Two-phase flow measurement technique*

The experimental technique used to characterize the dispersed phase was particle Doppler analysis. The equipment selected for this task was an Aerometrics Phase Doppler Particle Analyser (PDPA). This system allows simultaneous measurements of the horizontal and vertical velocities, as well as of the diameter of the particles. Two beams, with wavelengths of 514 nm (green) and 488 nm (blue), from a Coherent I70 2-C Ar^+ continuous laser are split and a frequency shift is introduced in one branch of each colour. The beams are then driven through optical fibres to a 250 mm focal length transmitting lens. The green beams are positioned in the horizontal plane and the blue ones in the vertical plane. The beams cross at a point of the flow materializing the probe volume, which is very small even compared with the Kolmogorov scale of the flow ($0.5 \times 0.5 \times 2.5\ \eta^3$). Any particle crossing the probe volume scatters the light which is received by the collecting optics located in the forward side at 30° from the emitter. This mode of operation, 30° forward first mode of refraction, has been shown to be the most advantageous for water droplets in an air flow, Bachalo (1994).

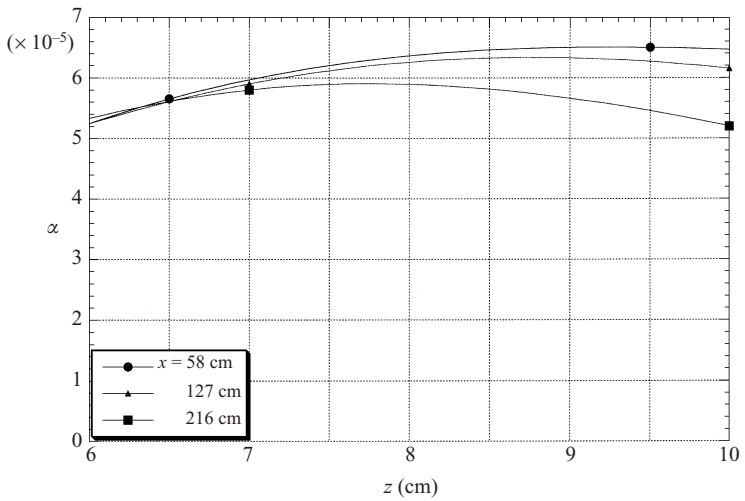

FIGURE 11. Local volume fraction profiles at different locations downstream. $y = 10\,\text{cm}$.

The velocity and size of the droplets are, then, computed from the frequency and phase-shift introduced by the droplets in the Doppler bursts. A complete description of the system, as well as a detailed study of the error in the measurements, can be found in Kiger (1995) and Kiger & Lasheras (1995). Since in the present work the turbulence is homogeneous and isotropic, no velocity bias correction due to large-scale structures is necessary. However, it is important to take into account the alignment errors introduced in the vertical velocity measurements by the fact that the laser beams can only be positioned in the vertical plane with finite precision. Since the horizontal velocity is two orders of magnitude larger than the vertical velocity, a small projection of the horizontal velocity measured by the vertical channel will create a significant error. This error is the same for all particles because the horizontal velocity is the same for all droplets (deviations are smaller than u'). This alignment bias can be effectively corrected by subtracting the measured vertical velocity of the smallest droplets in the lowest volume fraction case, whose average vertical velocity should be zero since they follow the flow, from all the vertical velocity measurements.

The uniformity of the droplet seeding was checked using a sampling technique. A thin tube, 10 mm in diameter, was introduced in the tunnel and positioned parallel to the main flow. The water flow rate collected by the tube was measured directly while the air flow rate was computed based on the tube diameter and the air velocity measured with one of the PDPA channels. Since the dispersed phase adopts the carrier flow axial velocity soon after injection, the volume fraction can be estimated by the ratio of the volumetric flow rates: $\alpha = Q_l/(Q_g + Q_l)$. As shown in figure 11, the sampling determined that the injection was uniform within 10% in a 4 cm region centred around the point where the measurements were taken ($z = 8\,\text{cm}$).

2.3. *Flow visualizations*

A high-resolution (1008×1016 pixels) digital camera was used to obtain images of the flow at several locations downstream of the particle injection. The flow is illuminated with a Continuum Surelite I 5 W pulsed Yag laser, whose light is directed through a cylindrical lens and a rectangular slit so that a very thin sheet of light is projected into the tunnel. The width of the sheet is approximately 1 mm (or 5η) so integration

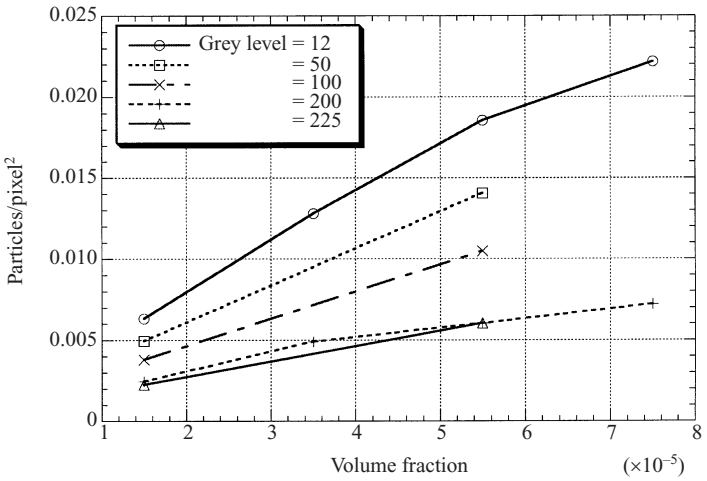

FIGURE 12. Average number of particles per pixel. Effect of the threshold.

in the direction perpendicular to the flow is minimized, and the duration of the pulses is 10 ns, short enough to freeze the motion of the droplets. The camera is mounted perpendicular to the laser plane and images of a 35 mm by 35 mm region of the flow are taken. The light scattered by the droplets is captured over a black background. The images are then processed to extract information about the spatial location of the particles in the flow.

Using NIH image processing software, the images were made binary and processed. By thresholding the data with different light intensities, the noise due to multiple reflections, current leekage from saturated pixels or microlense spreading can be rejected. However, strict thresholds reject small particles which create dim reflections in the images. The sensitivity of the measurements to the threshold was systematically analysed and found to be negligible in the range used in our experiments. The number of droplets per image, which can be observed in figure 12, decreases as the threshold is raised, as could be expected. However, the number of droplets in an image increases linearly with the volume fraction which ensures that the statistics based on the relative concentration, C/C_0, are unbiased.

During the image processing, each particle is reduced to a single pixel located at its centroid. A representative raw image and its processed binary image are shown in figure 13, where the presence of preferential accumulation of particles can be observed. Information on the preferential accumulation of particles obtained with this processing method is presented in § 3.2.

3. Experimental results

Simultaneous measurements of the size and vertical velocity of the droplets were taken 100 and 200 cm downstream from the injection grid. Large data sets (10^6 droplets) were acquired for each water mass loading. The data were divided into eleven bins, according to the diameter of the droplets. Each bin was characterized by the Stokes number computed using the average diameter in the bin. At the $x = 100$ cm downstream station, where most of the experimental data were collected, particles with a diameter of 30 μm have a Stokes number equal to 1 and a corresponding terminal velocity ratio equal to 0.6.

(*a*)

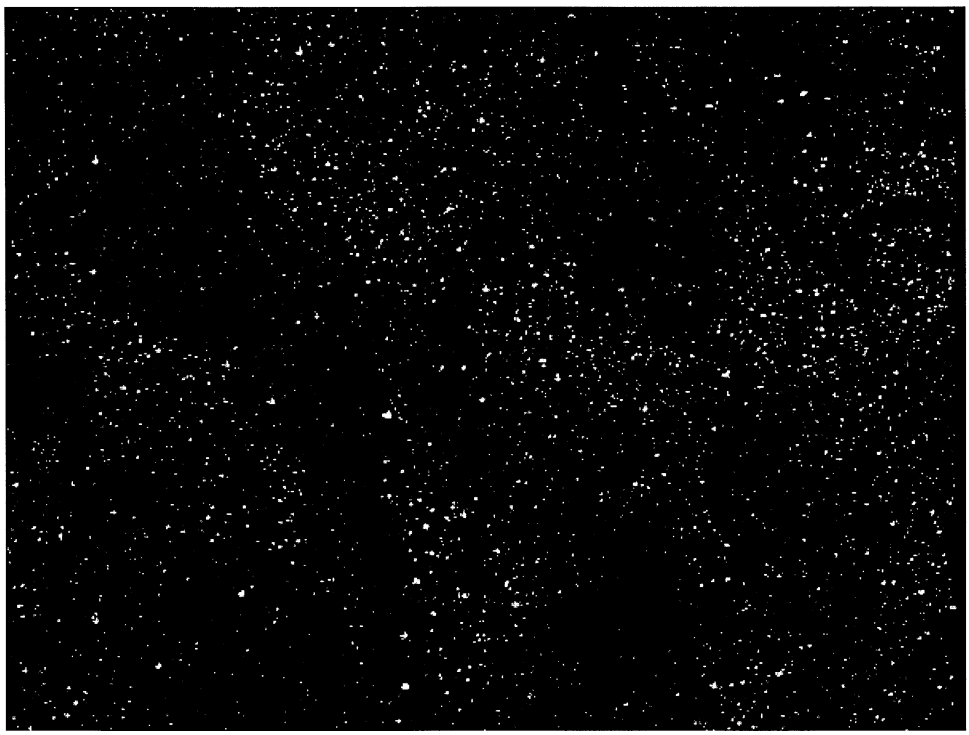

(*b*)

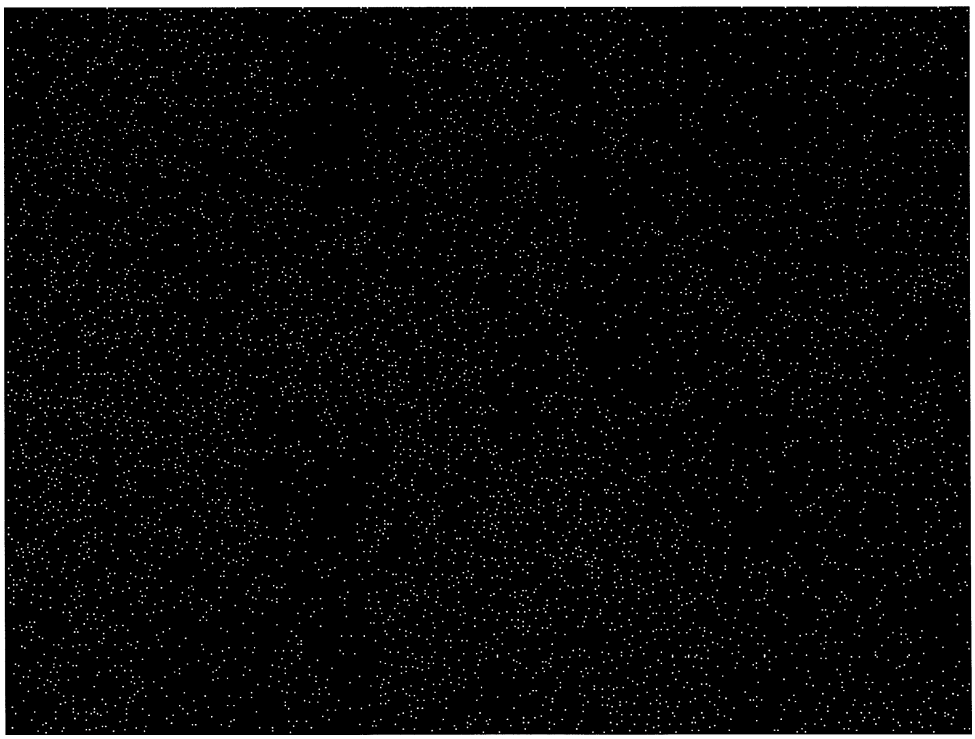

FIGURE 13. Flow visualizations. (*a*) Raw image. (*b*) Processed binary image.

3.1. *Enhancement of the settling velocity*

In this section we report the measurements of the mean vertical velocity of the droplets and its dependence on both the turbulence characteristics and the droplet volume fraction.

The instantaneous vertical velocity of all particles in each size class was averaged to compute the mean value of the settling velocity of particles of that size. This settling velocity is computed in an Eulerian sense, by averaging measurements of different particles taken at a fixed point. The Lagrangian settling velocity measured by following the trajectory of a particle is also of interest, but unfortunately could not be computed in this study where the number of particles present in the flow is too large to track individual ones. The settling velocity of particles in a still fluid, hereafter called the Stokes velocity (V_{St}), is subtracted from the averaged settling velocity measured, and the difference is non-dimensionalized with the RMS of the carrier flow (u'). This dimensionless quantity has been proposed by Wang & Maxey (1993) to characterize how the turbulence enhances the settling velocity of particles of different sizes. Plots of the non-dimensional increase of the settling velocity at two different downstream locations, as a function of the Stokes number, are shown in figure 14.

Results for different values of the droplet mass loading or, equivalently, dispersed-phase volume fraction (α) show the same qualitative behaviour. The variation of the increase in the settling velocity with the Stokes number is similar for all cases, exhibiting a maximum in the neighbourhood of $St \approx 1$. There is also a common tendency to decay to zero as the Stokes number becomes either zero or infinity. This can be easily explained by considering that the Stokes number measures the tuning of the response time of the particle to the excitation by the turbulence. Particles with Stokes number equal to one have the optimal sensitivity to the inertial bias caused by the turbulence. Very big particles, with large Stokes numbers, fall through the turbulent structures without responding to their fluctuations in velocity, due to their large inertia and short interaction time. Very small particles, on the other hand, have very small inertia (very small Stokes numbers) and long interaction time, and they follow the flow completely. Thus, their *average* settling velocity is zero. The PDF of the velocity measurements was found to be close to a Gaussian distribution, see figure 15. This seems to discard any possible bias in the sampling and indicates that the velocity enhancement is statistically significant for all the particles, so the mean velocity is a good measure of the long-time settling behaviour of the particles.

The magnitude of the enhancement of the velocity was, however, found to be very different for the different values of the particle volume fraction studied. When the volume fraction increases, the settling velocity enhancement increases, and this was found to be true throughout the entire range of Stokes numbers at both downstream locations. To better appreciate this trend, we show in figure 16 the non-dimensional settling velocity increase plotted versus the droplet volume fraction in the flow, with the Stokes number as a parameter. It is apparent from this plot that there is a monotonic increase in the settling velocity enhancement with the volume fraction of droplets in the flow. It must be emphasized that the range of volume fractions used in all the experiments reported here is such that the turbulence is not significantly affected by the presence of the particles, Eaton (1994), Elghobashi & Truesdell (1993), so this mechanism of turbulence modification by high particle volume fractions can be discarded as the mechanism responsible for the observed enhancement vertical velocity in V_z.

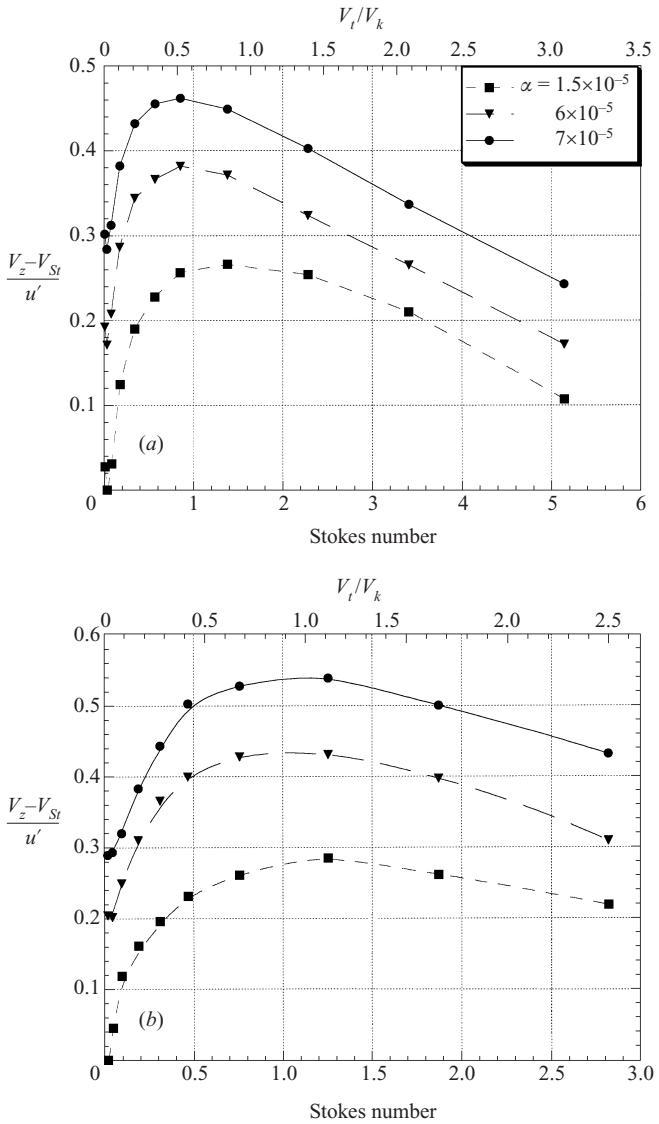

FIGURE 14. Increase in the settling velocity of particles as a function of their Stokes number, for different volume fractions. (*a*) $x = 100$ cm. (*b*) $x = 200$ cm.

3.2. *Clustering of particles due to turbulence*

Turbulence has the effect of preferentially concentrating heavy particles, producing spatially non-homogeneous distributions, even if the particles are homogeneously injected into the flow. This effect, which leads to the formation of high local concentration regions, known as clusters, has been well documented by the numerical simulations of Squires & Eaton (1991), Wang & Maxey (1993) and Yang & Lei (1998), among others, and has been experimentally observed in monodisperse systems by Fessler, Kulick & Eaton (1994). The relation between the preferential concentration of particles and their settling velocity enhancement has been investigated in the present study.

To study the characteristic dimensions of the clusters in the flow, the local concen-

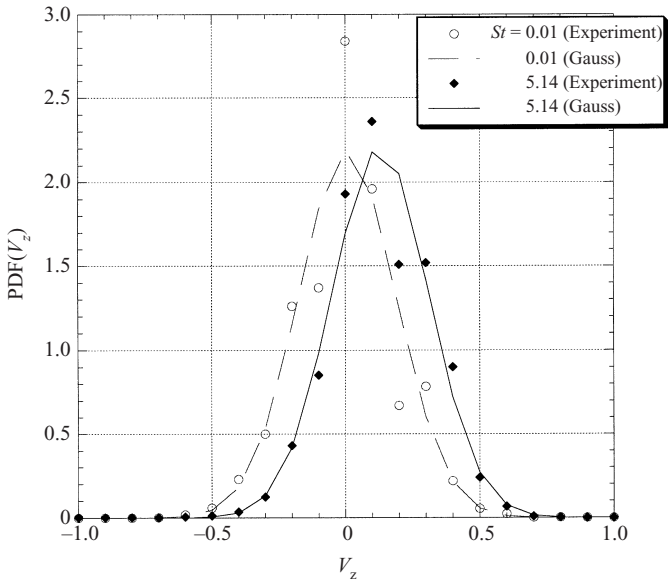

FIGURE 15. Probability density function of the vertical velocity measurements. $\alpha = 7.510^{-5}$, $x = 100\,\text{cm}$.

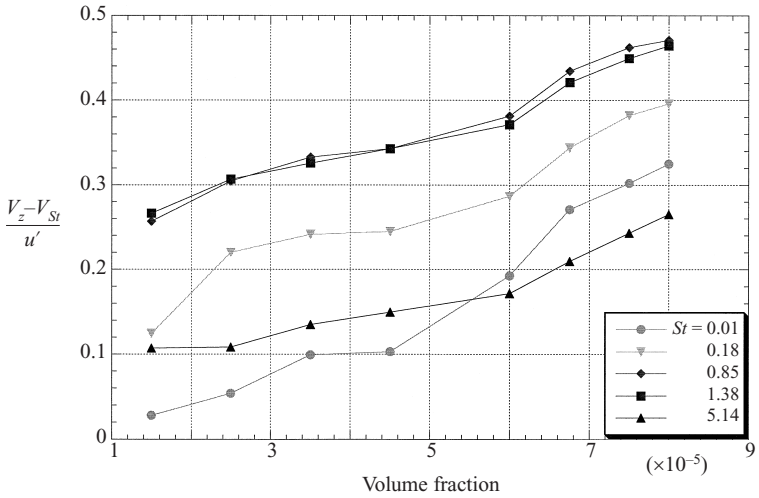

FIGURE 16. Effect of the volume fraction on the settling velocity enhancement, for different particle sizes. $x = 100\,\text{cm}$.

tration probability density function can be compared with that arising from a purely random process. Images of horizontal and vertical cross cuts of the flow were taken at different locations downstream from the injection point. The concentration PDF was obtained by dividing an image into boxes of a certain size and counting the number of particles inside each box (figure 17). The distribution of particles in boxes for a random process is given by a binomial distribution:

$$P_{binom}(n) = \binom{N_p}{n} \left(\frac{1}{N_b}\right) \left(1 - \frac{1}{N_b}\right)^{N_p - n}. \tag{3.1}$$

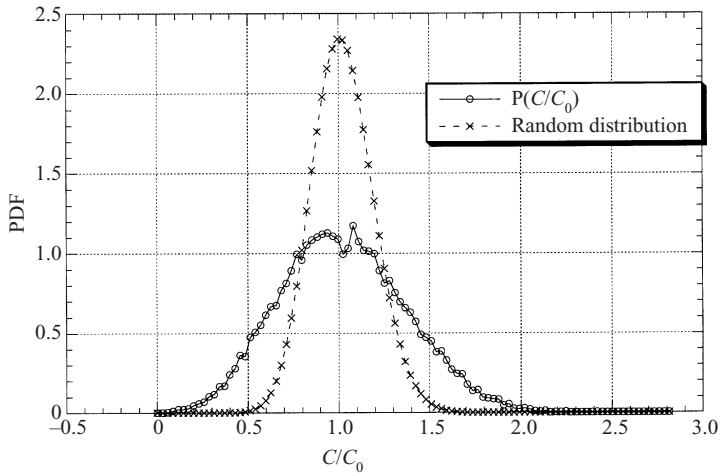

FIGURE 17. Probability density function of the number of particles per box. Total number of particles N_p, number of boxes N_b, $C_0 = N_p/N_b$.

This distribution tends to a Poisson distribution, when both the number of particles and the number of boxes tend to infinity:

$$P_{poisson}(n) = \frac{\mathrm{e}^{-\lambda}\lambda^n}{n!}, \tag{3.2}$$

where λ is the mean number of particles per box, N_p/N_b, and $P(n)$ is the probability of finding n particles in a box. For large volume fraction cases where the number of particles is too large to compute the binomial distribution analytically, we used (3.2).

The comparison between the PDF found for a given box size and the random process provides us with an indication of how turbulence affects the particle concentration field. We have used two parameters to compare the measured PDF to the random distribution. The first one, D_1, was introduced in Fessler *et al.* (1994), and is the difference between the standard deviation of the two distributions:

$$D_1 = \frac{\sigma - \sigma_{binom}}{\lambda}. \tag{3.3}$$

Positive values of this parameter indicate the presence of concentrated regions, while negative values represent a quasi-uniform concentration field that is close to a Dirac's delta probability distribution. The second parameter, D_2, was used by Wang & Maxey (1993) to analyze their DNS results. It represents the square of the difference of probabilities given by the two distributions:

$$D_2 = \sum_{n=1}^{N_p} (P(n) - P_{binom}(n))^2. \tag{3.4}$$

It is, by definition, always positive or zero.

The length scale for which preferential concentration is most effective can be identified by computing these statistics for boxes of different sizes. Figure 18 shows the results of computing these two parameters, D_1 and D_2. It can be seen that both reach a maximum value at the same location. Furthermore, we also found that this result is insensitive to the details of the processing, namely the threshold. The maximum was consistently located at values of the box size around 10η, for

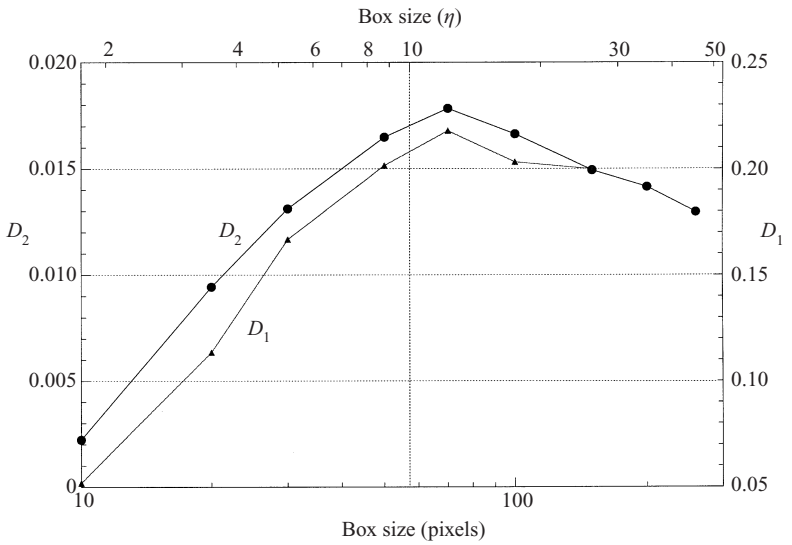

FIGURE 18. Two estimates of the difference between the PDF of particles in the flow and that of a random process. Evolution with the length scale.

all volume fractions used in the experiments. The suggested scaling of the location of the maximum with η seems to indicate that a characteristic length scale for the regions where particles accumulate due to turbulence (clusters) should be related to the smallest scales of the flow. Therefore, particle clusters seem to be under the influence of viscous effects.

In order to achieve a better understanding of the structure of the clusters, local concentration maps were produced by counting the number of particles inside a circle centred at each point. The radius was fixed at 3η which was found to be a good compromise between the spatial resolution and accuracy of the concentration measurements. An example of these concentration maps is shown in figure 19. Within these maps there are regions of very high concentration, relative to the mean. Determining the extent of these regions is of major importance in quantifying the influence of local concentration on the settling velocity. Clusters are hereafter defined from iso-concentration contours, as regions where the concentration is higher than a prescribed level. In parallel with the analysis of scalar mixing of Catrakis & Dimotakis (1996), these will be referred to as level sets. The objects identified from this analysis are then characterized by their perimeter, P, their area, A, and the concentration level, $C_{cluster}$. The relationship between the perimeter and the area of the clusters is shown in figure 20. When the perimeter of the clusters is plotted versus the square root of the area, both scaled with η, one can observe two different behaviours. When the structures of the clusters are small and 'compact', P and $A^{1/2}$ are linearly related, whereas larger cluster structures exhibit a fractal nature. This fractal nature has been reported previously by Hogan, Cuzzi & Dobrovolskis (1999), from numerical simulations, and by Fessler *et al.* (1994), from experiments. These features were found to be always present for the different level sets studied. Thus, one can conclude that either the perimeter or the area can be used, in a first approximation, to characterize the dimension of the clusters. We have used the area in figure 21 to study the occurrence of clusters in the flow. The number of structures of a given size was computed for a set of images, at different levels of concentration. For a given level set, the number of clusters of a given area was found to decay exponentially with size. Moreover, the argument

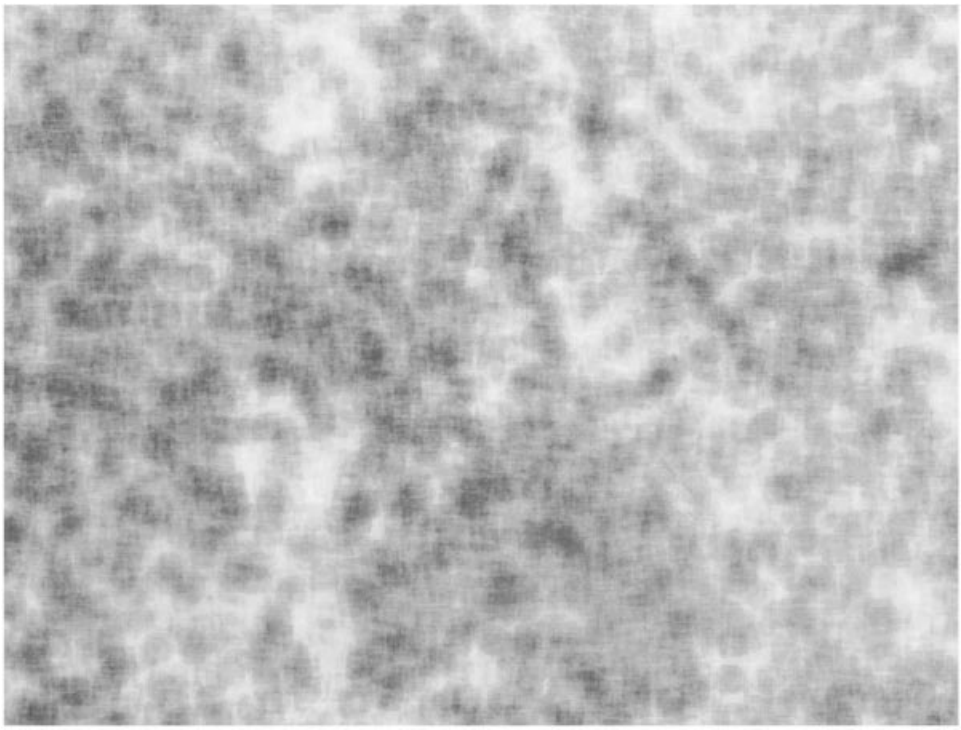

FIGURE 19. Local concentration map. From the image shown in figure 13.

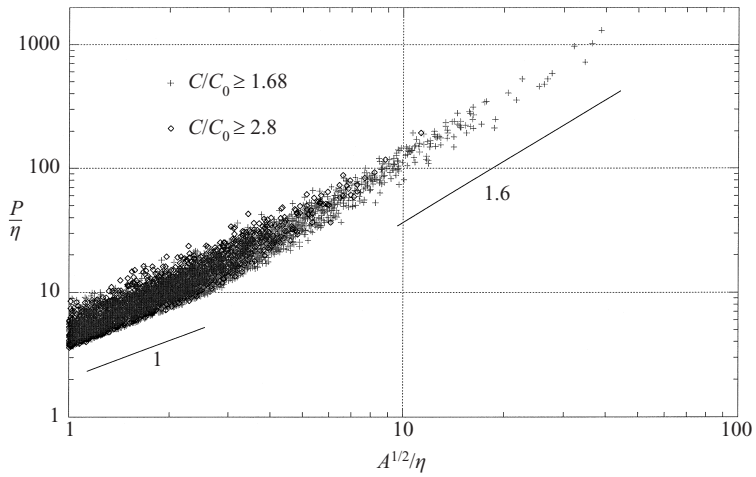

FIGURE 20. Perimeter vs. square root of the area of clusters for two different level sets.

of the exponential was found to increase with the concentration, indicating that the dimension of the clusters decreases drastically as the concentration level is increased.

Another important measure of the dimensions of the cluster can be obtained by examining the environment that the particles find. By computing the cumulative number of particles contained in regions of a certain size and concentration, the cluster thickness as seen by the particles can be estimated. Figure 22 shows such a

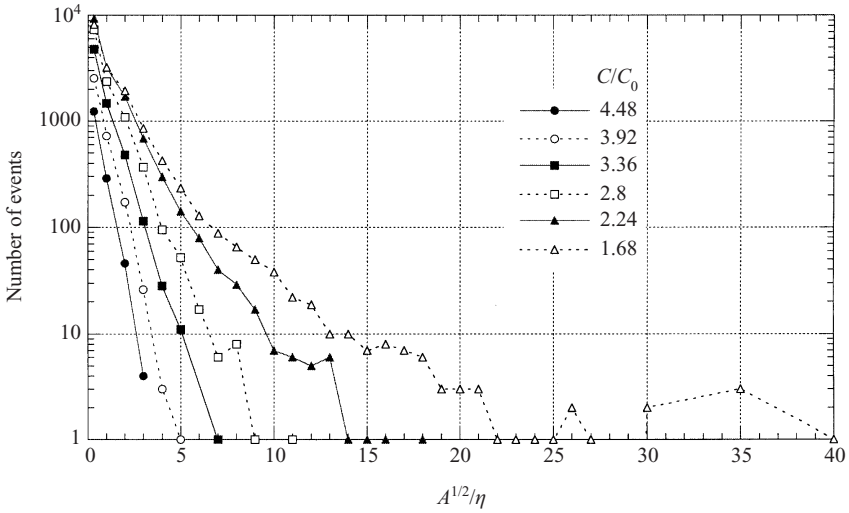

FIGURE 21. Number of clusters of a given area, for different concentration levels. Volume fraction $= 5 \times 10^{-5}$. $x = 100$ cm. 30 images processed.

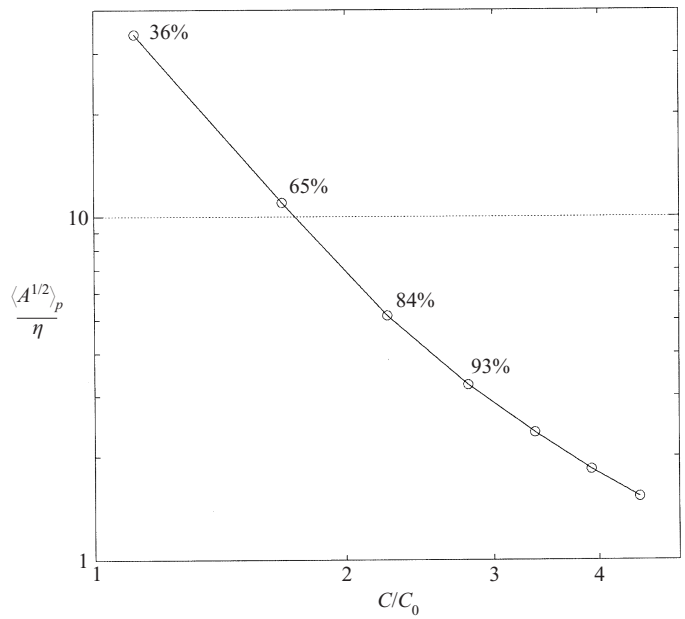

FIGURE 22. Typical cluster thickness as seen by the particles.

plot. It can be observed that about 50% of all particles are found in regions with a characteristic thickness between 7η and 16η and where the concentration is between 1 and 2.5 times the mean. This information strongly supports the finding that the significant thickness for particle accumulation regions is of the order of 10η.

3.3. *Measurements of the settling velocity of the particles conditioned to the local concentration*

Measurements of the local concentration of particles in the flow were also obtained from the PDPA data presented earlier in this section. The PDPA data consist of four

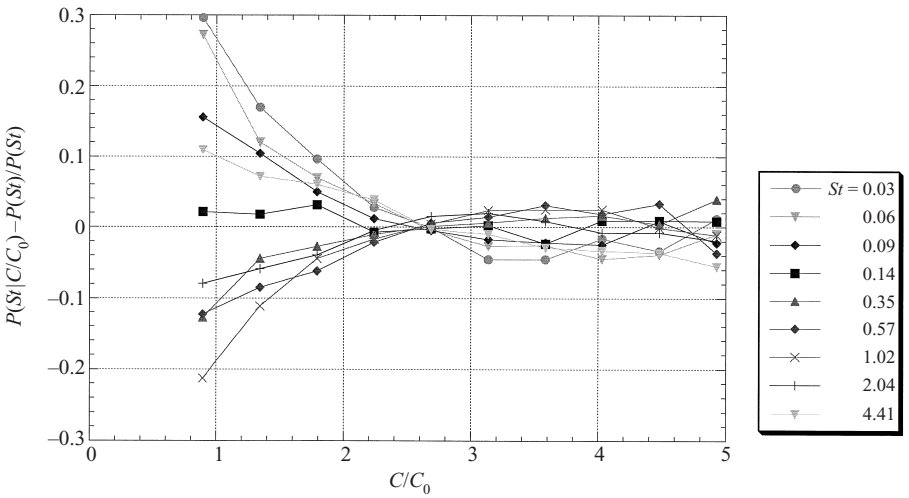

FIGURE 23. Preferential concentration of particles, for different Stokes number. Size PDF conditioned on the local concentration, compared to the overall size PDF of the flow. $x = 100\,\text{cm}$, $\alpha = 7.5 \times 10^{-5}$.

fields recorded for each droplet that crosses the interrogation volume. Those fields are: diameter, horizontal velocity, vertical velocity and time of arrival. The positions where the measurements were taken are at a sufficient distance downstream from the injection point to ensure that all droplets have reached the horizontal velocity of the flow with fluctuations smaller than or equal to those of the single-phase flow ($\approx 2\%$ of the mean). Therefore, the inter-arrival time between particles can be related to the inter-particle distance by using the mean horizontal velocity of the flow. The local concentration around a particle can then be computed by counting the number of particles that are within a given distance of the particle of interest. However, PDPA concentration measurements suffer from several effects that bias these results, making it extremely difficult to obtain absolute concentrations, Sommerfeld & Qiu (1995). Thus, we did not attempt to conduct these measurements. Instead, the experimental settings were optimized for maximum data rate while preserving the proportionality with the droplet volume fraction. In this way reliable relative concentration, C/C_0, measurements were obtained. Using the information from the image processing about the size of the preferential concentration regions, the number of particles within 10η of each particle were counted. Particles were classified according to the number density found around them and statistics were computed for these groups.

In figure 23 we plot the probability of finding particles of a given size in a region of a certain local concentration compared to the probability of finding a particle of that size over the entire flow. Observe that particles with $St \approx 1$ accumulate more efficiently and are less likely to be found in regions of low concentration, whereas small and large particles are found in those regions in proportions larger than the average. The opposite is true for high-concentration regions, although the difference in relative probabilities is much smaller. The composition of the clusters is very similar to the injected distribution, the probability of finding particles with $St \approx 1$ is slightly increased and the probability of particles with $St \ll 1$ or $St \gg 1$ is slightly decreased. Those small probability surpluses and deficits found in high-concentration regions balance the larger differences in probability at lower concentration, where the number of particles is much smaller.

The same conditioning technique was used to process the vertical velocity data.

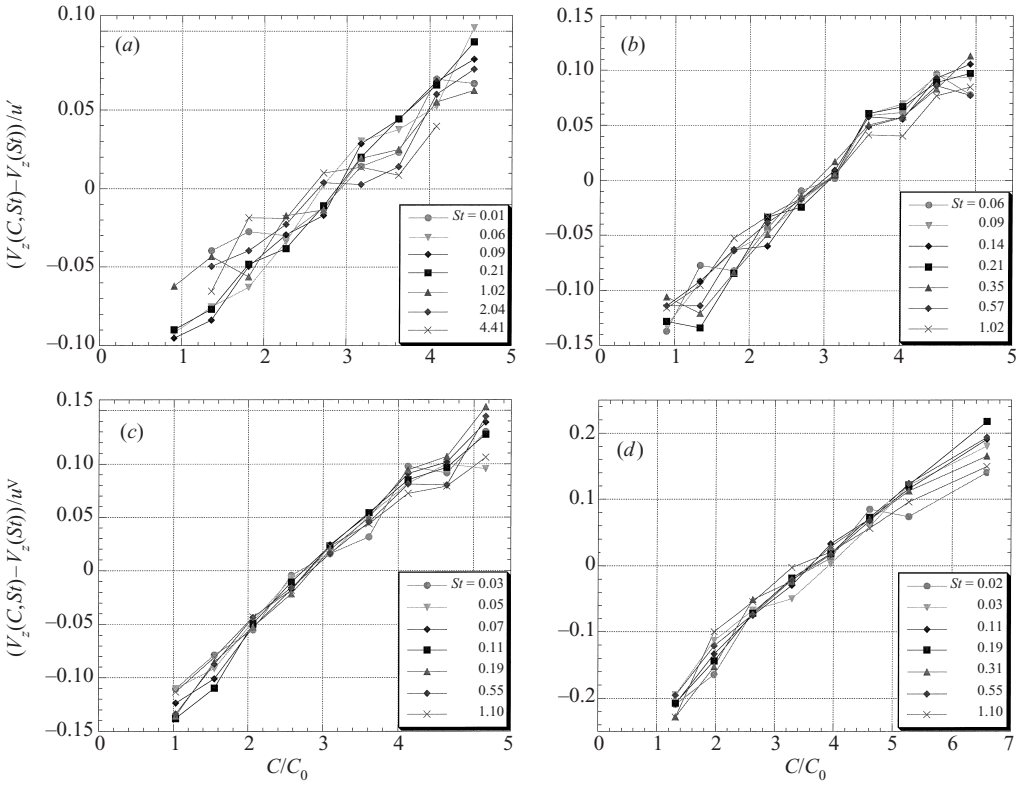

FIGURE 24. Enhancement of the settling velocity as a function of the local concentration. (*a*) $x = 100\,\text{cm}$, $\alpha = 6 \times 10^{-5}$. (*b*) $x = 100\,\text{cm}$, $\alpha = 7.5 \times 10^{-5}$. (*c*) $x = 200\,\text{cm}$, $\alpha = 5 \times 10^{-5}$. (*d*) $x = 200\,\text{cm}$, $\alpha = 7.5 \times 10^{-5}$.

Averaging the vertical velocity of all particles found in regions of a given concentration, the influence of the local concentration on the settling velocity of particles was studied. Figure 24 shows the results from this processing for two different volume fractions of particles at downstream locations $x = 100\,\text{cm}$ and $x = 200\,\text{cm}$. The difference between the averaged settling velocity of particles of a given size conditioned by a given concentration and the velocity of particles of that same size class averaged over all concentrations is plotted versus the local concentration. The tendency of the settling velocity to increase as the local concentration increases is evident, and this dependence is almost linear, within the range studied. The fact that curves for all sizes collapse indicates that the mechanism responsible for this increase is most probably a collective effect.

4. Analysis and discussion of the results

The experimentally determined settling velocity enhancement of particles in a turbulent flow, shown in figure 14, exhibits all the qualitative features shown in the DNS of Wang & Maxey (1993). As in Wang & Maxey's simulation, the vertical velocity enhancement plots have a well-defined maximum consistently located near $St \approx 1$. There are, however, quantitative differences between the values measured in our experiment and the ones computed in Wang & Maxey's simulation. It has to be kept in mind that the simulations were done without any mechanism by which one

particle could feel the presence of the others, thus they can only be compared to our results in the limit of zero volume fraction. Furthermore, the simulations were done at Reynolds numbers lower than our experiment, and they showed a weak dependence of the settling velocity enhancement on Re_λ. However, considering these differences, the simulations compare well with the measurements in the smallest volume fraction case. For the higher volume fractions, the experimental values of the increase in the settling velocity are significantly larger than the simulated ones. Since, for the range of concentrations used, the enhancement in the experimentally determined settling velocity increases monotonically with the volume fraction in the flow, we explored the possibility that the preferential accumulation of particles could be responsible for this behaviour. This in turn would explain the discrepancy with the simulations where the increase in the settling velocity due to turbulence is computed without any influence of the particles on each other, and is independent of the volumetric fraction of particles in the flow.

We have already mentioned that the maximum increase of the settling velocity is always found for particles whose Stokes number is close to one. This supports the scaling argument we introduced when we defined the Stokes number in terms of the Kolmogorov velocity. On the other hand, we cannot shed any new light on which should be the correct scale for the velocity increase. Although we have chosen to scale it with u' and the resulting non-dimensional increase varies only slightly as the flow conditions change between $x = 100\,\text{cm}$ and $x = 200\,\text{cm}$, the velocity scales u' and V_k evolve similarly as the turbulence decays, as seen in table 1. Unfortunately, there is not enough dynamic range in our experiments to study which would be the correct scale for the settling enhancement.

Results from the two different downstream locations are very consistent. The main difference between the conditions at these two stations is that, as the turbulence dissipation rate decays, the ratio V_t/V_k decreases compared to the Stokes number of the particles. In the $x = 200\,\text{cm}$ case, particles with $St \approx 1$ also have $V_t/V_k \approx 1$ and the value of the maxima are found to be larger than in the $x = 100\,\text{cm}$ case, where the maximum occurs at $V_t/V_k \approx 0.5$. This influence of the terminal velocity ratio, although weak, agrees with the previous findings that suggest values of V_t/V_k between 1 and 2 as optimum for the settling velocity enhancement.

Despite the random nature of turbulence, the distribution of particles in a turbulent flow is far from random. In fact, it exhibits large intermittency in the temporal and spatial concentration fields. Inertial bias creates a tendency for heavy particles to accumulate in regions of high strain rate and low vorticity. This tendency induces the creation of clusters of particles and those clusters are denser and more numerous as the volume fraction of particles in the flow increases. Both tendencies are supported by our experimental findings, namely in figure 24 the value where the lines cross the abscissa (local concentration for which the velocity corresponds to the average velocity) is larger for larger volume fractions.

Clusters are regions of relatively high concentration formed when particles accumulate in regions of low vorticity and high strain. As a number of particles come close enough they start to interact through the surrounding fluid, and no longer react to the turbulence independently. This region where the particles locally perturb the flow and interact with each other is what we call a cluster. Once formed, the cluster continues to settle, entraining other particles. Those particles will see their vertical velocities enhanced and they will increase the relative density of the cluster, thus increasing its settling velocity. Eventually, the interaction with another turbulent structure will disperse the particles, ending this feedback process. The effect of these regions on

the overall statistics of the flow is negligible, so they cannot be revealed in two-way coupling simulations by considering turbulence modulation. However, this collective effect might be recovered in those simulations by studying the local perturbations of the carrier fluid velocity inside these high-density regions, possibly through the modification of the pressure field.

Previous studies of preferential accumulation have been carried out in flows with mono-dispersed distributions of particles. These studies predict an important difference between accumulation of particles with Stokes number near one and those with Stokes number far from unity. The results in figure 23 show a significant difference in the low-concentration regions. However, as the local concentration increases, the difference disappears. The particle size distribution in our experiment is poly-dispersed and so the different behaviour could very well be explained if we consider that in this case particles of $St \approx 1$ accumulate preferentially and form clusters which then entrain particles of all sizes. In flows with mono-dispersed distributions, either all particles tend to accumulate, which makes the accumulation more evident, or they all tend towards a random distribution and clusters do not form. This hypothesis is consistent with the fact that the maximum values found in figure 18, where the spatial distribution is compared with a random one, are smaller than the values obtained when all particles are of the same size, Wang & Maxey (1993) and Fessler *et al.* (1994).

In figure 21 we noted that the largest cluster areas are about 15η for $C/C_0 > 2.2$, and 7η for $C/C_0 > 3.4$, which is fully consistent with the maximum occurrence of clustering at 10η shown in figure 18. However, that figure showed the presence of elongated structures, and thus of larger characteristics sizes. As the level of complexity in the description of the cluster structure increases, the analysis becomes more difficult. In figure 21 we observe that most of the clusters, especially those with higher concentrations levels, have an equivalent radius equal to or less than 10η. Also, in figure 20, one can observe that the clusters that most significantly affect the settling velocity are within the range where the perimeter and the square root of the area are linearly related.

When the cluster size calculated from the image processing was used to conditionally average the vertical velocity, we found a quasi-linear behaviour characterized by two parameters: the slope and the value at $C/C_0 \to 0$. The settling velocity that particles would have in isolation can be computed using the mean velocity from figure 14 and the slope and mean cluster concentration from figure 24:

$$V_{is}(St) = \overline{V_z(St, \alpha)} - \frac{\mathrm{d}V_z}{\mathrm{d}C/C_0}(\alpha) C/C_0(\alpha)|_{V_z = \overline{V}_z} \tag{4.1}$$

The results are shown in table 2. These values can be compared with numerical simulations and with experimental data in the limit of very small volume fraction. The comparison between the settling velocity for isolated particles ($St \approx 1$) predicted from the data in figures 14 and 24 and the measured velocity for the smallest volume fraction, from figure 14, is shown in table 2. The values found for isolated particles in high volume fraction flows, are remarkably similar to the mean settling of particles in the lowest volume fraction case (taken to be the limit in which the settling velocity of one particle is not influenced by the presence of other particles). This indicates that particles only perceive the local concentration in their vicinity and that they are unaware of the overall volume fraction in the flow, as long as the properties of the turbulence are not significantly altered. The slope of the settling velocity as a function of relative concentration can be related to the dynamics of the clusters. Table 3 shows

x (cm)	Volume fraction	$\frac{V_{is} - V_{St}}{u'}$	$\frac{\overline{V_z}(\alpha_{min}) - V_{St}}{u'}$
100	6×10^{-5}	0.24	0.26
	7.5×10^{-5}	0.27	0.26
200	5×10^{-5}	0.26	0.28
	7.5×10^{-5}	0.26	0.28

TABLE 2. Settling velocity of isolated particles. $St \approx 1$.

		From the model	From figure 24	
x (cm)	α	$\frac{V_{cl}/u'}{c/c_0}$	$\frac{\mathrm{d}V_z/u'}{\mathrm{d}C/C_0}$	$C/C_0(V_z = \overline{V_z})$
100	6×10^{-5}	0.051	0.052	2.81
	7.5×10^{-5}	0.063	0.065	3.05
200	5×10^{-5}	0.053	0.068	2.95
	7.5×10^{-5}	0.074	0.102	3.84

TABLE 3. Settling velocity dependence on the local concentration. Comparison between model and experiments.

the values of the slopes obtained when a linear fit is applied to the plots in figure 24. A preliminary effort to relate those values to the behaviour of the clusters is made in the next section.

5. A phenomenological model of the effect of preferential accumulation on the settling velocity of the particles

As mentioned in the introduction, it is already well known that particles accumulate on the downward side of the eddies and that their settling velocity is enhanced. This has been called the preferential sweeping effect and it has been well established both theoretically and from DNS results, Wang & Maxey (1993). However, if preferential sweeping were the only effect, the increase in the settling velocity of particles would be independent of the number of particles in the flow, as long as that number were not large enough to attenuate the intensity of the turbulence or to promote collisions. Our experimental results shown in figures 14 and 16 clearly indicate that there is a dependence of the enhancement of the velocity on the volume fraction of particles in the flow. If particle accumulation becomes more important as more particles are added to the flow and the enhancement of the settling velocity also becomes larger as the volume fraction increases, it is reasonable to hypothesize that there ought to be a correlation between the formation of particle clusters and the settling velocity of the particles.

It could be argued that the velocity increase with the local concentration is just an effect of the correlation between the regions of high concentration and the downward side of the eddies. Particles in regions of high concentration are also most likely to be on the downward side of the eddies and, when averaged, the resulting settling velocity is larger than the overall mean. This argument, which arises from the point

of view of particles interacting with an isolated, horizontal vortex, fails to explain the phenomenon when turbulence is isotropic and eddies do not have a preferential orientation. Moreover, the increase with the volume fraction cannot be explained by this argument.

The idea that clusters play an important role in the settling of particles, supported by the result shown in figure 16, led us to develop a simple phenomenological model to estimate the settling velocity of particles, while inside a cluster, as the sum of two terms:

$$V_z = V_{is} + V_{cluster}. \tag{5.1}$$

The first term is the settling velocity that isolated particles would have in a turbulent flow. This term is formed by the Stokes velocity that particles would have in a quiescent fluid plus the enhancement due to the preferential sweeping by turbulence. It can be observed in the limit of very low volume fraction of particles in the flow and has been computed in direct numerical simulations, Wang & Maxey (1993).

The second term in the equation is due to the effect that clusters have on the settling velocity of particles inside them. In order to estimate this second effect, which has not been addressed before, we model the clusters as large pseudo-particles with a characteristic size l and a mean density ρ_{cl} given by the local concentration of particles in them, $\rho_{cl} = (1 - c)\rho_{air} + c\rho_p$. Further assuming that clusters are inside the viscous domain (the Reynolds number of the clusters is at most of order 10), the interaction with the surrounding carrier fluid can be expressed in the form of a simple Stokes drag law. The equilibrium between the weight of the cluster and the drag exerted by the fluid will give us an estimate of the terminal velocity of the cluster as a function of its concentration:

$$(\rho_{cl} - \rho_{air})\frac{\pi l^3}{6} g = \tfrac{1}{2}\rho_{air} V_{cl}^2 \frac{\pi l^2}{4} C_D, \tag{5.2}$$

where V_{cl} is the settling velocity of the cluster.

The velocity of the clusters is then

$$V_{cl} = \frac{K_T}{18}\frac{\rho_p}{\rho_{air}}\frac{g}{\nu_{air}} C l_{cl}^2, \tag{5.3}$$

where K_T depends on the volumetric shape factor, Clift, Grace & Weber (1978), and it ranges between 0.3–0.5 for long and thin structures, and equals 1 for spheres. It is important to note the linear dependence of this expression on the local concentration of particles, confirmed by the experimental results from figure 24. Thus, we can rewrite equation (5.1) as $V_z = V_{is} + mC/C_0$, where m corresponds then to $\mathrm{d}V_z/\mathrm{d}C/C_0$. Using the experimental value of l_{cl}, the characteristic length of the clusters, one can estimate the ratio between the cluster velocity and the RMS of the flow velocity as a function of the relative concentration, that is the value of m. Despite the simplicity of the model, the results shown in table 3 are comparable to the experimentally determined slopes of the curves in figure 24, also given in the table.

The data in table 3 can be used to estimate the effect of clustering on the mean settling velocity of particles. According to this simple model, since the particle size PDF inside the clusters is roughly the same as in the overall flow, the effect is the same for particles of all sizes. That can be compared with the increase due to the volume fraction. Subtracting the settling velocity of the smallest volume fraction from the values for larger volume fractions in figure 14 also gives an estimate of how much of the increase in the settling velocity is due to clustering. Figure 25 shows those estimates for the four different cases in table 3. The model gives a good prediction

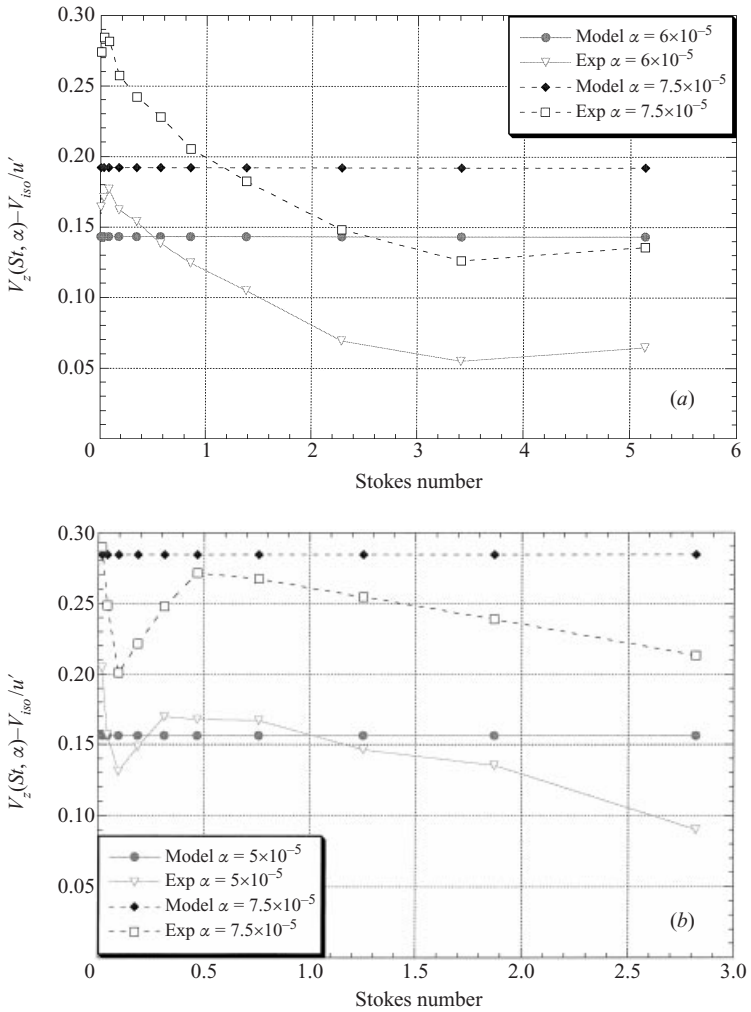

FIGURE 25. Effect of clusters on the increase in the settling velocity of particles as a function of their Stokes number. Comparison between model and experiments. (*a*) $x = 100$ cm, (*b*) $x = 200$ cm.

of the effect for particles of $St \approx 1$, but overpredicts the effect for large particles and underpredicts it for small particles. The predictions are in good agreement with the experimental data, especially for the data taken at $x = 100$ cm, which is where we measured the size of the clusters. However, the underestimate of the slope at $x = 200$ cm may be due to the evolution of the cluster characteristic length, which has been assumed to be constant at all locations and equal to 10η, an assumption which needs further study.

It is worth noting that the proposed model does not provide the unconditional settling velocity. The fraction of time that a given particle remains under the influence of clusters is not known. One should introduce an intermittency factor, γ, to express the unconditional settling velocity as

$$\overline{V_z(St,\alpha)} = V_{is}(St) + \int \gamma(St,\alpha,C)V_{cl}(C)\,\mathrm{d}C. \tag{5.4}$$

Extracting γ from the above expression requires accounting for the variability in the cluster structure, and such detailed information is not available from the experiments.

If equation (5.4) is compared to equation (4.1), we can understand the value of $C/C_0(\alpha)|_{V_z=\overline{V_z}}$ as an integrated measure of the intermittency factor. The value of this parameter, the local concentration where the mean settling velocity is reached, is shown in table 3 to vary from case to case, increasing with the volume fraction.

6. Conclusions

Experiments have been conducted to study the behaviour of heavy particles in homogeneous, isotropic, decaying turbulence. We have shown that the settling velocity of the particles is enhanced by the turbulence, and the concentration field shows large inhomogeneities. We attribute these to the preferential sweeping and the preferential concentration of particles by the turbulent structures, effects that have been predicted theoretically and simulated numerically but for which very scarce experimental evidence had been found so far. The use of the Kolmogorov scales to formulate the parameters that govern the problem is supported by the location of maxima for values of the Stokes number and the terminal velocity ratio of order one. The correct scaling for the increase of the settling velocity is still an open question.

We have studied the concentration field of particles in the flow by means of image processing. Digital images of the flow have been taken and analysed in an effort to characterize the geometry of the concentration field. The comparison of the distribution of the number of particles in boxes of a certain size and the distribution in a random process (binomial/Poisson) has unveiled a length scale where the concentration is most correlated. This length scale has been determined to be $O(10\eta)$ and can be interpreted as a characteristic cluster length. This result is in very good agreement with length scales for preferential accumulation found in previous experiments, Fessler *et al.* (1994).

Although there are important questions about the clusters that are still open, namely the characteristic size, shape and lifetime, we have made an initial analysis of the particle clustering and the results are encouraging.

We also found a dependence of the settling velocity enhancement on the particle volume fraction that cannot be explained in terms of the behaviour of isolated particles in a turbulent flow. We then proposed a new mechanism to explain the effect of the number density of particles on the settling velocity of a neighbouring particle. Conditional measurements of the settling velocity as a function of the local concentration of particles support the hypothesis that regions of high concentration are formed and behave as large pseudo-particles that we call clusters. These clusters settle in the lower-density fluid surrounding them with their own velocity, which adds to the settling velocity of the particles inside them. By comparing the velocity conditioned on the local concentration with the unconditional velocity, and scaling them with a characteristic velocity of the flow, be it u' or V_k, we showed that all the measurements collapse. The result is a straight line for particles of all sizes, whose value at the origin gives the settling velocity of isolated particles, and whose slope gives the effect of clustering on the settling velocity of particles.

Finally, we proposed a simple phenomenological model to address this behaviour. The terminal velocity of clusters is computed using the characteristic cluster length found and assuming Stokes drag is applicable, and that value, which depends linearly on the local concentration, is added to the velocity of isolated particles. Given the simplicity of the model the predictions are in good agreement with the experiments, both in predicting the trend with the local concentration and in the mean effect that clustering has on the enhancement of the settling velocity with droplet volume fraction.

Refinements of the model accounting for the shape complexity of the clusters and dependence of the size PDF on the local concentration could be studied to increase accuracy.

This work was supported by the ONR through grant N00014-96-1-0213 and NASA under the Microgravity Fluid Mechanics Program. The first author is indebted to the La Caixa Foundation for a Graduate Fellowship.

REFERENCES

Auton, T. R., Hunt, J. C. R. & Prud'Homme, M. 1988 The force exerted on a body in inviscid unsteady nonuniform rotational flow. *J. Fluid Mech.* **197**, 241–257.

Bachalo, W. D. 1994 Experimental methods in multiphase flows. *Intl J. Multiphase Flow* **20**, Suppl., 261–295.

Boivin, M., Simonin, O. & Squires, K. D. 1998 Direct numerical simulation of turbulence modulation by particles in isotropic turbulence. *J. Fluid Mech.* **375**, 235–263.

Catrakis, H. J. & Dimotakis, P. E. 1996 Mixing in turbulent jets: scalar measures and isosurface geometry. *J. Fluid Mech.* **317**, 369–406.

Clift, R., Grace. J. R. & Weber, M. E. 1978 *Bubbles, Drops and Particles*. Academic.

Comte-Bellot, G. & Corrsin, S. 1966 The use of a contraction to improve the isotropy of grid-generated turbulence. *J. Fluid Mech.* **25**, 657–682.

Crowe, C. T., Troutt, T. R. & Chung, J. N. 1996 Numerical model for two-phase turbulent flows. *Annu. Rev. Fluid Mech.* **28**, 11–43.

Druzhinin, O. A. 1995 On the two-way interaction in two-dimensional particle-laden flows: the accumulation of particles and flow modification. *J. Fluid Mech.* **297**, 49–76.

Druzhinin, O. A. & Elghobashi, S. 1999 On the decay rate of isotropic turbulence laden with microparticles. *Phys. Fluids* **11**, 602–610.

Eaton, J. K. 1994 Experiments and simulations on turbulence modification by dispersed particles. *Appl. Mech. Rev.* **47**(6), part 2, 44–48.

Eaton, J. K. & Fessler, J. R. 1994 Preferential concentration of particles by turbulence. *Intl J. Multiphase Flow* **20**, Suppl., 169–209.

Elghobashi, S. & Truesdell, G. C. 1993 On the two way interaction between homogeneous turbulence and dispersed solid particles. I: Turbulence modification. *Phys. Fluids* **7**, 1790–1801.

Fessler, J. R., Kulick, J. D. & Eaton, J. K. 1994 Preferential concentration of heavy particles in turbulent channel flow. *Phys. Fluids* **6**, 3742–3749.

Février, P., Simonin, O. & Legendre, D. 2001 Direct and Large-eddy simulations of isotropic homogeneous turbulence. *Proc. 4th ICMF, 2001, New Orleans, USA*.

Hinze, J. O. 1975 *Turbulence*. McGraw-Hill.

Hogan, R. C., Cuzzi, J. N. & Dobrovolskis, A. R. 1999 Scaling properties of particle density fields formed in simulated turbulent flows. *Phys. Rev.* E **60**, 1674–1680.

Gañán-Calvo, A. M. & Lasheras, J. C. 1991 The dynamics and mixing of small spherical particles in a plane free shear layer. *Phys. Fluids* A **3**, 1207–1217.

Kiger, K. T. 1995 Particle dispersion and inter-phase kinetic energy transfer in a turbulent, two phase shear layer. PhD thesis, University of California, San Diego.

Kiger, K. T. & Lasheras, J. C. 1995 Effect of vortex pairing on particle dispersion and inter-phase kinetic energy transfer in a two phase turbulent shear layer. *J. Fluid Mech.* **302**, 149–178.

Kulick, J. D., Fessler, J. R. & Eaton, J. K. 1994 Particle response and turbulence modification in fully developed channel flow. *J. Fluid Mech.* **277**, 109–134.

Lasheras, J. C. & Tio, K. K. 1994 Dynamics of a small spherical particle in steady two-dimensional vortex flows. *Appl. Mech. Rev.* **47**, 6, part 2, 61–69.

Lázaro, B. J. & Lasheras, J. C. 1992*a* Particle dispersion in the developing free shear layer. Part 1. Unforced flow *J. Fluid Mech.* **235**, 143–178.

Lázaro, B. J. & Lasheras, J. C. 1992*b* Particle dispersion in the developing free shear layer. Part 2. Forced flow *J. Fluid Mech.* **235**, 179–221.

MAXEY, M. R. 1987*a* The motion of small spherical particles in a cellular flow field. *Phys. Fluids* **30**, 1915–1928.

MAXEY, M. R. 1987*b* The gravitational settling of aerosol particles in homogeneous turbulence and random flow fields. *J. Fluid Mech.* **174**, 441–465.

MAXEY, M. R. & RILEY, J. J. 1983 Equation of motion for a small rigid sphere in a nonuniform flow. *Phys. Fluids* **26**, 883–889.

NIR, A. & PISMEN, L. M. 1979 The effect of a steady drift on the dispersion of particles in a turbulent fluid. *J. Fluid Mech.* **94**, 369–381.

RUETSCH, G. R. & MEIBURG, E. 1993 On the motion of small spherical bubbles in two-dimensional vortical flows. *Phys. Fluids* A **5**, 2326–2341.

SCHRECK, S. & KLEIS, J. S. 1993 Modification of grid-generated turbulence by solid particles. *J. Fluid Mech.* **94**, 665–688.

SNYDER, W. H. & LUMLEY, J. L. 1971 Some measurements of particle velocity autocorrelation function in turbulent flow. *J. Fluid Mech.* **48**, 41–71.

SOMMERFELD, M. & QIU, H. H. 1995 Particle concentration measurements by phase-Doppler anemometry in complex dispersed two-phase flows. *Exps. Fluids* **18**, 187–198.

SQUIRES, K. D. & EATON, J. K. 1990 Particle response and turbulence modification in isotropic turbulence. *Phys. Fluids* A **2**, 1191–1203.

SQUIRES, K. D. & EATON, J. K. 1991 Preferential concentration of particles by turbulence. *Phys. Fluids* A **3**, 1169–1178.

SUNDARAM, S. & COLLINS, L. R. 1999 A numerical study of the modulation of isotropic turbulence by suspended particles. *J. Fluid Mech.* **379**, 105–143.

TIO, K. K., GAÑÁN-CALVO, A. M. & LASHERAS, J. C. 1993 The dynamics of small, heavy, rigid spherical particles in a periodic Stuart vortex flow. *Phys. Fluids* A **5**, 1679–1693.

TRUESDELL, G. C. & ELGHOBASHI, S. 1994 On the two way interaction between homogeneous turbulence and dispersed solid particles. II. Particle dispersion. *Phys. Fluids* **6**, 1405–1407.

WANG, L. P. & MAXEY, M. R. 1993 Settling velocity and concentration distribution of heavy particles in homogeneous isotropic turbulence. *J. Fluid Mech.* **256**, 27–68.

WELLS, M. R. & STOCK, D. E. 1983 The effect of crossing trajectories on the dispersion of particles in a turbulent flow. *J. Fluid Mech.* **136**, 31–62.

YANG, C. Y. & LEI, U. 1998 The role of the turbulent scales in the settling velocity of heavy particles in homogeneous isotropic turbulence. *J. Fluid Mech.* **371**, 179–205.